Photoelectron Spectrum Of Inorganic Solids In Gas Phase

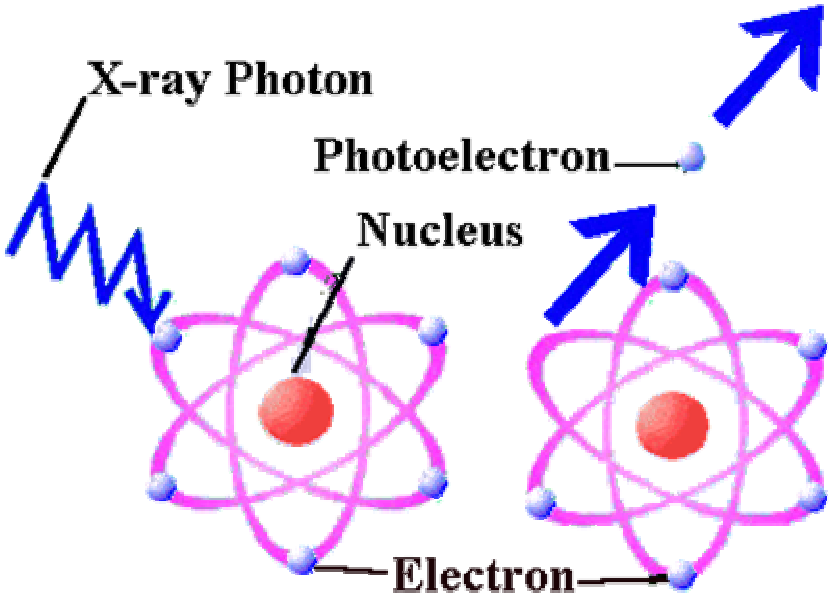

Sumanta Kumar Meher
CY05D040
V. Velkannan
CY05D035

Introduction:

This is a spectroscopic technique which measures the kinetic energy of electrons emitted upon the ionization of a substance by high energy monochromatic photons. A photoelectron spectrum is a plot of the number of electrons emitted versus their kinetic energy. The spectrum consists of bands due to transitions from the ground state of an atom or molecular entity to the ground and excited states of the corresponding radical cation. Approximate interpretations are usually based on 'Koopmans theorem' and yield orbital energies. PES and UPS (UV photoelectron spectroscopy) refer to the spectroscopy using vacuum ultraviolet sources, while ESCA (electron spectroscopy for chemical analysis) and XPS use X-ray sources.

The XPS technique involves the bombardment of a sample surface with X-rays and the measurement of the concomitant photoemitted electrons. The photoemitted electrons have discrete kinetic energies that are characteristic of the emitting atoms and their bonding states. XPS goes beyond elemental analysis to provide chemical information. It can be distinguish chemical arrangements such as silicon-to-silicon bonds and silicon-to-oxygen bonds.

Gas-phase PES is a powerful tool for probing metal ligand covalency in isolated molecules because the relative ionization intensities observed in a PE spectrum are dependent upon the incident photon energy. This technique gives a picture of the molecular orbital energies and, consequently, insight into the bonding and reactivity of complexes. This shows the difference in molecular and electronic structure between the free molecule and the solid state. Problem is associated with intermolecular interactions in the solid phase and is not as useful for understanding reactivity as are the valence ionizations that are much more closely related to thermodynamic cycles and the orbitals associated with the reactivity of molecules. Gas phase measurements are particularly important for comparison to computational results because other spectroscopic methods are often affected by solution or other intermolecular interactions.

Experimental :

The gas phase XPS experiment is conducted in an apparatus consisting of a laser vaporization source, a time-of-flight mass spectrometer and a magnetic bottle photoelectron spectrometer. Negative ion photoelectron spectroscopy is conducted by crossing a mass-selected beam of anions with a fixed frequency photon beam and energy analyzing the resultant photodeteched electrons. The ion source consists of a Smalley-style laser vaporization source which utilizes a pulsed gas valve, a rotating and translating sample rod made of an aluminum/lithium alloy, and second harmonic light pulses from an Nd: YAG laser. Most of these electrons are then energy analyzed by a magnetic bottle photoelectron spectrometer and detected with a multi channel plate. This technique is governed by the following energy-conserving relationship:

$$h\nu = \text{EKE} + \text{EBE}$$

Where $h\nu$ is the photon energy,
EKE is the measured electron kinetic energy, and
EBE is the electron binding energy.

Just before the anions passes through the ion–photon interaction region, they encounter a mass gate followed by a momentum decelerator. Immediately after the ion–photon interaction region, a Channeltron electron multiplier monitors the arrival of the ions. At the ion–photon interaction region, electrons are photo detached from the anion of interest with the third harmonic of a second Nd:YAG laser. Most of these electrons are then energy analyzed by a magnetic bottle photoelectron spectrometer and detected with a multichannel plate. A LeCroy digital oscilloscope collects the data, which is manipulated with a laboratory computer

The optical layout of the pump and probe beams :

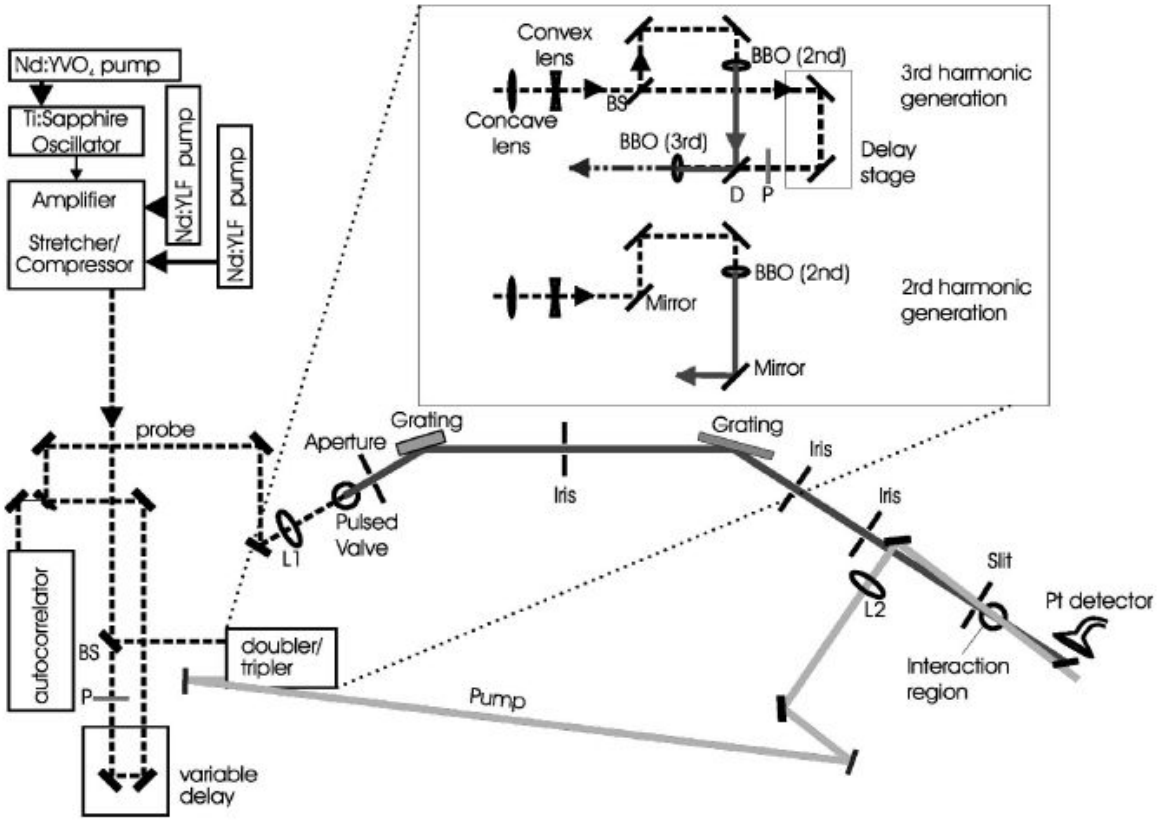

The optical layout of the pump and probe beams. The output beam is split into pump and probe beams at the 80/20 beamsplitter. The 20% reflected beam is sent into the doubler/tripler to frequency upconvert the pulse to 400 or 266 nm. The pump beam then passes through a 70 cm lens ~L2! Into the chamber, and after reflection from the mirror inside the vacuum chamber, comes to a focus between the slit and the interaction region ~focal position variable! The 400 nm beam has an 50 mm focal diameter, with a maximum intensity in the interaction region of ;1013 W/cm^2 ~dependent on focal position!. The transmitted beam ~80%! passes through a half-wave plate ~*P*! and a delay stage and is then focused with a 40 cm lens ~L1! into the pulsed gas jet. The selected harmonic is directed and focused into the interaction region. The 17th harmonic, as an example, is focused to a; 200 mm diam spot with an estimated maximum intensity of 1.43108 W/cm^2 in the interaction region.

Inset: **First the pump beam is sent through a telescope to reduce the beam size. For second harmonic generation, the 800 nm beam is sent through a BBO crystal. For third harmonic generation, the 800 nm beams is split into 2 beams where one arm is doubled in a BBO crystal and combined again with the second 800 nm arm in a BBO crystal cut for summation to produce a 266 nm output.**

A detailed schematic of the spectrophotometer used in the analysis of inorganic solids in gas phase is shown here :

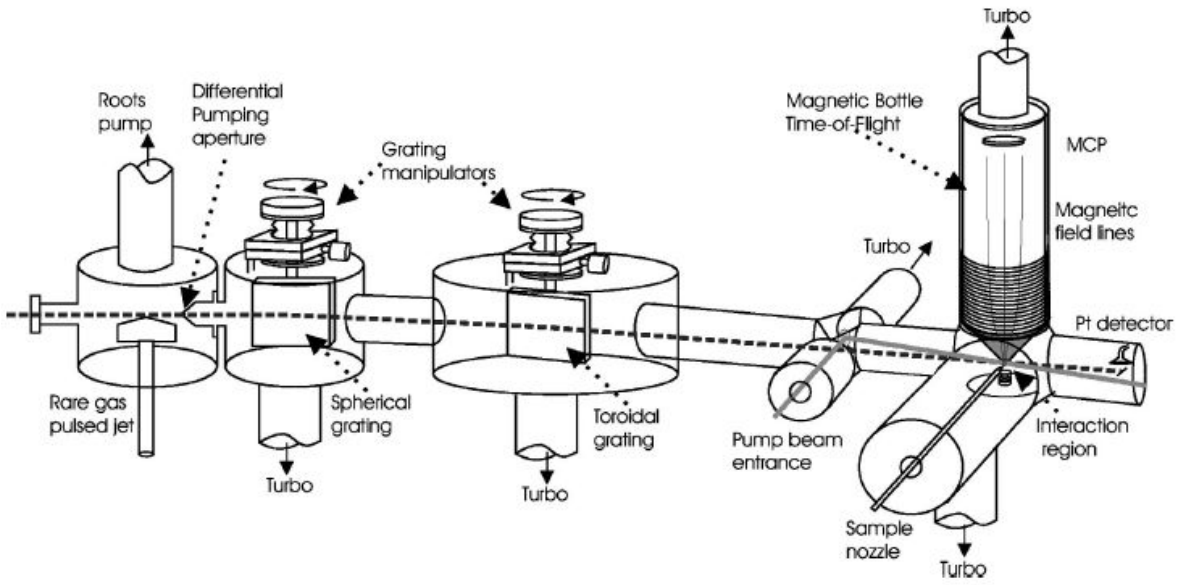

Here shown the pulsed valve chamber, the two grating chambers, and the magnetic bottle photoelectron spectrometer. The probe laser beam is focused into the pulsed valve gas jet where the harmonics are created. The harmonic of choice diffracts in first order off of the first concave grating, then again off the toroidal grating, and enters the interaction region where it intersects the gaseous sample. Ejected photoelectrons are collected in the magnetic bottle time-of-flight and detected with the MCP detector. The pump beam enters the chamber and reflects off of a mirror located slightly above the harmonic beam and crosses the harmonic beam at a small angle in the interaction region

Discussions of some inorganic solids in the gas phase

ZrO_2^- and HfO_2^- have been studied with photoelectron spectroscopy:

Zirconia (ZrO_2) and Hafnia (HfO_2) are of great interest due to their potential applications on microelectronics, catalysis, and ceramic materials. They are also important for our understanding of the role of d-electrons and f-electrons in chemical bonding. Zirconium and hafnium come from different periods on the periodic table, hafnium atom has f-orbitals while zirconium does not, however, it is known that hafnium and zirconium have very identical chemical properties due to the effect of the lanthanide contraction. Theoretical calculations, FTIR spectra and microwave spectra of ZrO_2 and HfO_2 show that they have similar M-O bond length and O-M-O bond angle (M=Zr, Hf), their vibrational frequencies are very similar, and their electric dipole moments are almost identical.

However, theoretical work on the relative stability of ZrO_2 and HfO_2 shows that the monoclinic baddeyelite phase of HfO_2 has a bulk modulus almost twice that of ZrO_2. Recent theoretical and experimental work found out that the thermodynamic stabilities of ZrO_2 and HfO_2 are quite different when they are in contact with silicon. Since thermodynamic stability is a very critical property that will affect their applications on making microelectronic devices, a clear understanding of this property is very necessary. As the geometric structures, vibrational and rotational states are not the main reasons that cause the difference between ZrO_2 and HfO_2; the main effects might come from their electronic structures. Detail information of their electronic states will be very useful for understanding the similarities or differences between ZrO_2 and HfO_2.

An experiment on photoelectron spectroscopy of ZrO_2^- and HfO_2^- in the gas phase is conducted because negative ion photoelectron spectroscopy is a very important tool to study the difference in the properties.

The measured electron affinity of HfO_2 is 2.14eV (±0.03eV), and the electron affinity of ZrO_2 is 1.64eV (±0.03eV).The coincidence between electron affinity and thermodynamic stability has been observed. This coincidence is due to the similarity of atomic and ionic radii of zirconium and hafnium atoms, and the difference of their electronic structures. Both the difference of thermodynamic stability and the difference of electron affinity are due to the same effects of pure electronic levels of ZrO_2 and HfO_2.

Both ZrO_2 and HfO_2 have been reported as C_{2v} structures with bond length around 1.77Å and bond angle around 108^o (R_{Zr-O}=1.7710Å, R_{Hf-O}=1.7764Å, bond

angle OZrO=108.11^{o}, bond angle OHfO=107.51^{o}). According to the photoelectron spectra, the measured vibrational frequency is 887±40cm^{-1} (0.11±0.005 eV) for both of them. This number is consistent with the matrix IR measurement of the symmetrical stretching mode (v_1) of those molecules (table 1).

The vibrational frequency of TiO_2's symmetric stretching mode (v_1) is measured to be 940cm^{-1}. ZrO_2 and HfO_2 have very similar vibrational frequencies while TiO_2 is different from them. It is also interesting to note that the atomic and ionic radii of zirconium and hafnium are very similar while those of titanium atom are different.

When the electron affinities (EA),are considered, the situation changes. The EA difference between TiO_2 and ZrO_2 is only 0.05eV (Table 1), however, the EA of HfO_2 is 0.50eV (48kJ/mol) higher than that of ZrO_2. Since hafnium atom has f-orbitals while titanium and zirconium do not, it indicates that the f orbitals play an important role in the formation of chemical bonds in HfO_2. Since the EA's are depending on the electronic structures, it supports the suggestion that electronic structure is the main thing that contributes to the difference of stability between ZrO_2 and HfO_2.

Table - 1
Electron Affinities and Vibration Frequencies for TiO_2, ZrO_2 and HfO_2

Electron Affinity		Vib. Freq. From PES	Vib. Freq from Matrix IR
TiO_2	1.59±0.03 eV	940±40 cm^{-1} (v_1)	946.9 cm^{-1} (v_1), 917.1 cm^{-1} (v_3)
ZrO_2	1.64±0.03 eV	887±40 cm^{-1} (v_1)	884.3 cm^{-1} (v_1), 818.0 cm^{-1} (v_3)
HfO_2	2.14±0.03 eV	887±40 cm^{-1} (v_1)	883.4 cm^{-1} (v_1), 814.0 cm^{-1} (v_3)

v_1- symmetric stretching, v_3- asymmetrical stretching, v_2- bending, v_2 is not shown here.

The spectrum of ZrO_2^- shows a main peak at 1.64eV corresponding to the transition from the ground state of ZrO_2^- anion to the ground state of ZrO_2 neutral. This implies the electron affinity of ZrO_2 is 1.64eV (±0.03 eV). The peaks at 1.75eV and 1.86 eV correspond to the vibrational structures of ZrO_2's electronic ground state. For the same reason, the main peak in the spectrum of HfO_2^- indicates the electron affinity of HfO_2 is 2.14eV (±0.03 eV). The spectrum is shown below

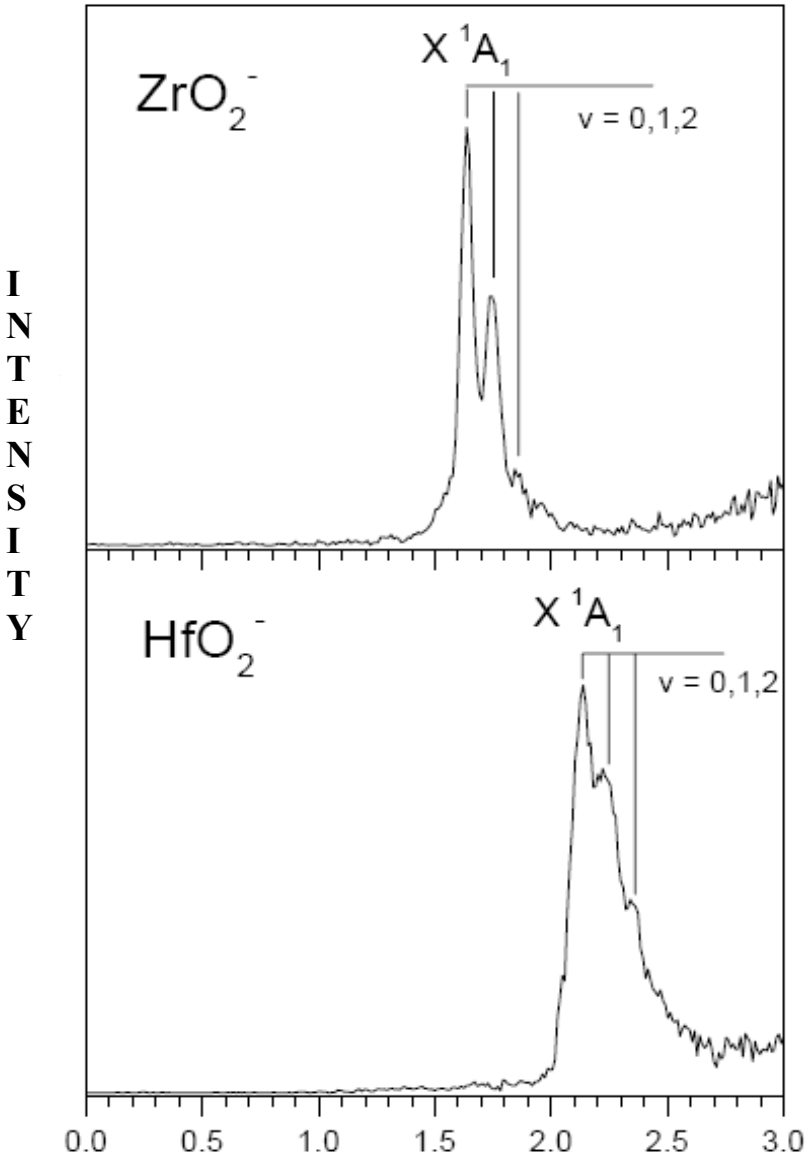

In conclusion, photoelectron spectroscopy study of ZrO_2^- and HfO_2^- anions is performed. By comparing ZrO_2 and HfO_2, it is found that the difference in their EA's coincides with the difference in their H_f's (enthalpies of formation). This is the first observation of the coincidence between electron affinity and thermodynamic stability.

Photoelectron spectroscopy study of SiO_2^- , SiO_3^- and SiO_4^- :

Silicon oxide is the most abundant substance on earth and is important in many technological areas. An understanding of the structure, bonding, surfaces, and defects in silicon oxide could aid development in diverse applications such as catalysis, amorphous materials, environmental sciences, and electronic device physics.

Photoelectron spectroscopy (PES) of size-selected $Si_xO_y^-$anions is used to obtain electronic and spectroscopic information of these clusters. The PES experiments yield unique structure and bonding information about the neutral clusters and allow systematic studies of a wide range of cluster sizes.

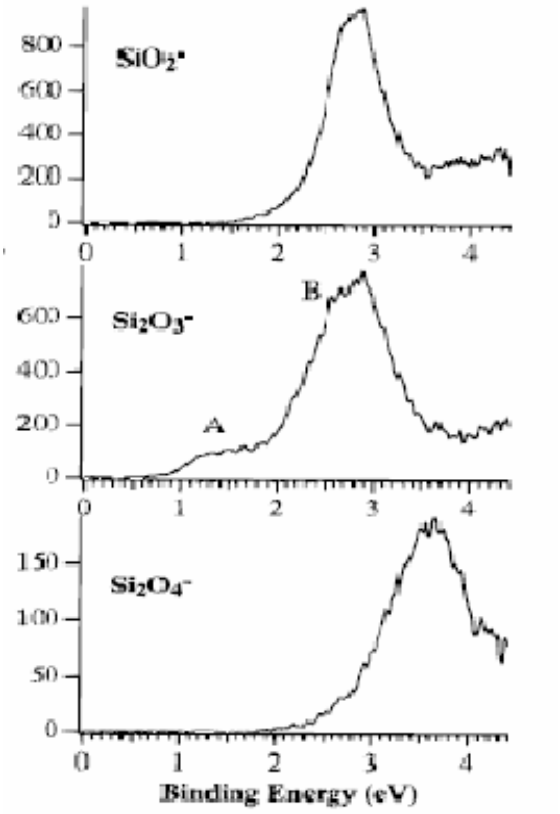

This figure (1) shows the PES spectra of SiO_2^-, $Si_2O_3^-$, and $Si_2O_4^-$ at 4.66 eV photon energy.

Only one broad band is observed for all the spectra except for that of $Si_2O_3^-$ which appears as two broad features, one at higher binding energy (labeled "B") and one weak feature at lower binding energy (labeled "A").

All of these species show quite low detachment cross sections, probably caused by the broad nature of the detachment transitions. Substantial low-energy electron noise (at high binding energies) was present due to the scattered photons.

These spectra represent photodetachment transitions from the ground state of the anion to the neutral states.

Si_2O_4 can be viewed as the dimer of SiO_2, and the dimerization energy have been estimated to be about 4.7 eV. However, the main vapor species of silica is the SiO diatomic. The Si_2O_4 molecule was first observed and studied in a matrix infrared experiment where it was formed by reacting Si_2O_2 with O_2. Its ground state structure is concluded to be a symmetric D_{2h} molecule with two terminal O atoms and two bridging O atoms (2,4 dioxocyclodisiloxane).

If we assume that the $Si_2O_4^-$ observed in our experiment corresponds to the D_{2h} neutral molecule, then the broad photoelectron spectrum shown in Figure 1 strongly suggests that there is a considerable geometrical change in the anion. Interestingly, a recent calculation on doubly charged $Si_2O_4^{2-}$ anion found that the two extra electrons enter an antibonding orbital and distorted the anion to a C_s structure, in which one terminal O atom is bent out of the molecular plane. It is expected that the singly charged anion should exhibit a similar distortion, as evidenced by our observed broad photoelectron spectrum.

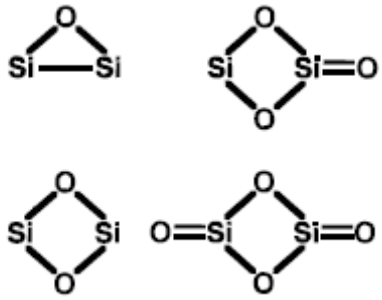

Figure (2) - Structures of the Si_2O_x (x = 1-4) clusters

The $Si_2O_3^-$ spectrum shows two broad features: one strong feature at higher binding energy ("B" in Figure 1) and one weak feature at lower binding energy ("A" in Figure 1) It should be noted that the feature "B" of $Si_2O_3^-$ is rather similar compared to that of SiO_2^-. This suggests that the feature "A" in the $Si_2O_3^-$ spectrum is most likely due to a different isomer.

The Si_2O_3 species can be viewed to be formed by removing an O atom from the Si_2O_4 molecule. There are two ways to do this, either removing a terminal O or a bridging O atom, giving two different Si_2O_3 structures. In reality, the Si_2O_3 species are probably the intermediate to form Si_2O_4 in the laser vaporization source. As a

matter of fact, the Si_2O_4 molecule formed from the reaction between Si_2O_2 and O_2 in the previous matrix experiment is most likely through such Si_2O_3 intermediates. The isotope substitution experiment using Si_2O_2 and isotopically labeled $^{18}O_2$ yields two isomers: ^{18}OSi(OO)Si^{18}O and ^{18}OSi-(^{18}OO) SiO, where the two O atoms in the parentheses indicate the bridging O atoms (Figure 2). The intermediates in the formation of these two Si_2O_4 isomers are consistent with the two Si_2O_3 isomers proposed above.

All the spectra show broad photo detachment features, suggesting that there is considerable geometry change between the anion and the neutral. The vertical detachment energies are determined to be 2.76 (0.10), 2.75 (0.10), and 3.63 (0.1) eV for SiO_2^-, $Si_2O_3^-$, and $S_{i2}O_4^-$, respectively. The spectrum of $Si_2O_3^-$ shows a weak feature at lower binding energy, suggesting existence of another isomer.

Electronic structure and chemical bonding of $MnCl_2$, $NiCl_2$, and $ZnCl_2$: A high resolution photoelectron spectroscopic study

A high temperature molecular beam source is needed to study these molecules with high resolution. Here the vibrational structures in the photoelectron spectra of these molecules are resolved .This provides important information about the chemical bonding and a better spectroscopic characterization of the molecular ions.

In experimental, the source used electron-bombardment heating and a graphite crucible, and it has the capability to entertain carrier gases to produce seeded supersonic beams of high temperature species with internal cooling.

The experimental condition is given in the following table:

	$ZnCl_2$	$MnCl_2$	$NiCl_2$
T(K)[a]	800	1000	960
P(Torr)[b]	110 (He)	120 (He)	500 (He)
ϕ(mm)[c]	0.18	0.23	0.16
Power (mA×V)[d]	30×600	200×600	60×1200
Starting materials	Pure $ZnCl_2$	Pure $MnCl_2$	Pure $NiCl_2$

[a] Accuracy of temperature measurements was ± 50 K.
[b] Carrier gas pressure.
[c] Nozzle diameters.
[d] Heating power, emission current (mA) times applied high voltage (V). About 60 W power was needed to drive the tungsten filament, which is in addition to the heating power.

The temperature control in vaporizing the samples is important.

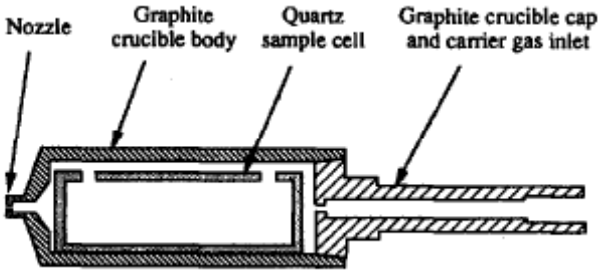

Here shown is the graphite crucible configuration with a sample cell.

We have the following valence electronic configuration for the ground state of $ZnCl_2$, $MnCl_2$ and $NiCl_2$

$$\cdots 1\delta_g^4 2\pi_g^4 8\sigma_g^2 9\sigma_g^2 7\sigma_u^2 4\pi_u^4 2\pi_g^4 \quad {}^1\Sigma_g^+ \quad ZnCl_2,$$
$$\cdots 8\sigma_g^2 7\sigma_u^2 4\pi_u^4 2\pi_g^4 1\delta_g^2 3\pi_g^2 9\sigma_g^1 \quad {}^6\Sigma_g^+ \quad MnCl_2,$$
$$\cdots 8\sigma_g^2 7\sigma_u^2 4\pi_u^4 2\pi_g^4 1\delta_g^4 3\pi_g^3 9\sigma_g^1 \quad {}^3\Pi_g \quad NiCl_2.$$

Photoelectron spectra of $ZnCl_2$:

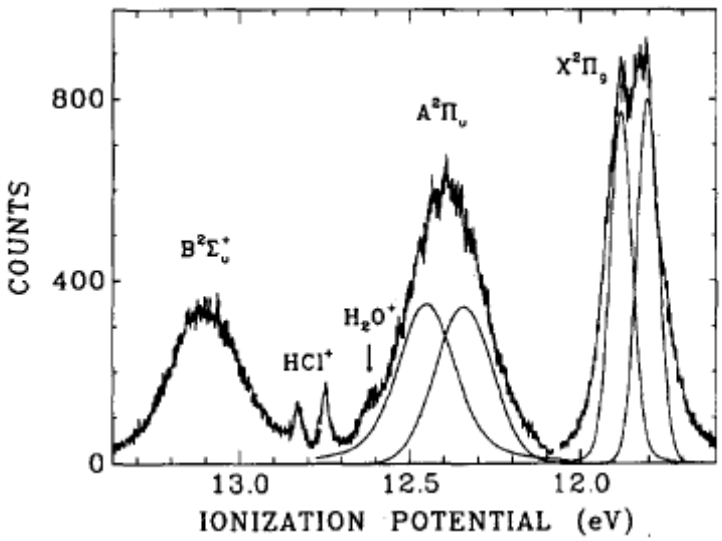

The He I photoelectron spectrum from the $2\pi_g$, $4\pi_u$ and $7\sigma_u$ orbitals of $ZnCl_2$ is shown above. Gaussians were fitted to the $A^2\Pi_u$ band and are plotted in the spectrum to show the spin-orbit components.

In the spectra, the spin-orbit splitting is partly resolved in the $X^2\Pi_g$ band, while the two spin-orbit components in the $A^2\Pi_u$ band are completely overlapped.

This is because the $4\pi_u$ orbital is a bonding orbital and has a broader Frank Condon envelope. For the $X^2\Pi_g$ band, the ν_2 mode is observed to be excited with frequency of about 240 and 260 cm^{-1} for the $^2\Pi_{g3/2}$ and $^2\Pi_{g1/2}$ components respectively. For the $A^2\Pi_{u3/2}$ band, two frequencies of 360 and 280 cm^{-1} are discernible. These are due to ν_1 and ν_2 modes respectively. Here a broad featureless band is observed for the $B^2\sum_u^+$ state. No vibrational structure is resolved in this band due to no complication in spin-orbit effect. This is due to the vibrational frequency becomes smaller in the $B^2\sum_u^+$ state and all three vibrational mode gets strongly excited.

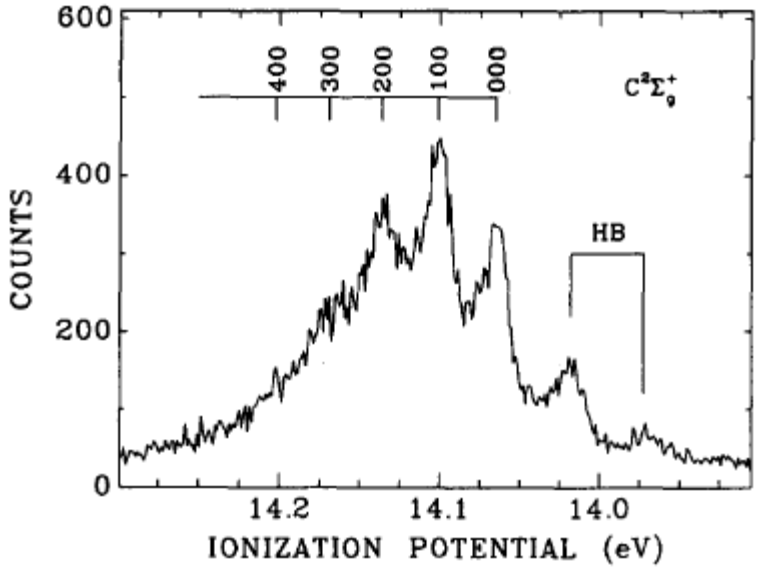

The He I photoelectron spectrum from the $9\sigma_g$ orbital of $ZnCl_2$ with the vibrational assignments. The vibrational levels are labeled with the ν_1, ν_2 and ν_3 vibrational quantum numbers. HB stands for the hot band transitions.

In the spectra, the first two peaks are assigned to hot band transitions. The rest of the spectrum is assigned to a ν_1 vibrational progression. The vibrational spacings are smaller than that in neutral ground state, indicating the strongly bonding character of the σ_g orbital.

Ionization potentials (eV) and assignments of the $C\,^2\Sigma_g^+$ state of $ZnCl_2^+$.

Ionization potential	Assignment[a]
13.975 (6)	Hot band ($\nu_1'' = 2 \rightarrow \nu_1' = 0$)
14.020 (5)	Hot band ($\nu_1'' = 1 \rightarrow \nu_1' = 0$)
14.065 (5)	0
14.101 (4)	1
14.136 (6)	2
14.170 (7)	3

[a] The ν_1 vibrational quantum number.

The figure below shows the comparison between calculated and experimental spectra

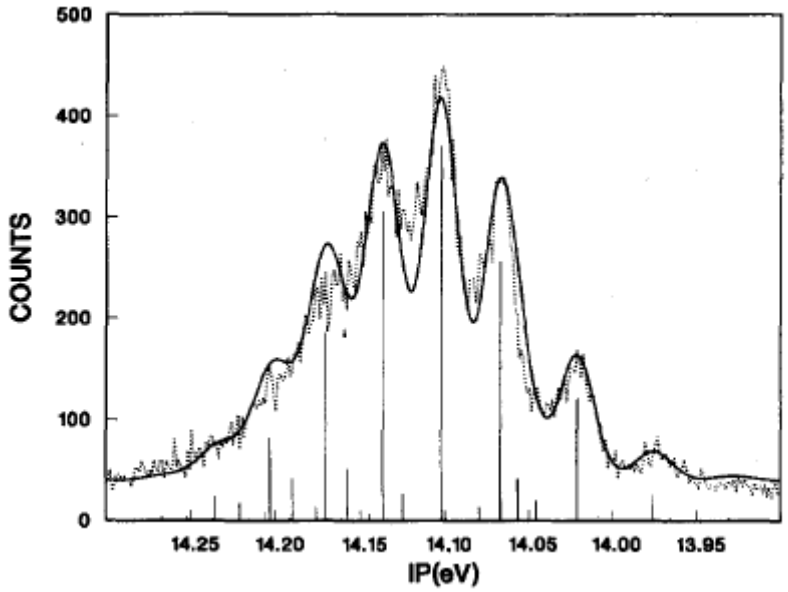

This is the comparison of a frank-Condon factor calculation With the $C^2\sum_g^+$ state experimental spectrum of $ZnCl_2^+$. The individual lines are the calculated Frank-Condon Factors, each of which is convoluted with a Gaussian (0.024 eV width) to compare to the experimental spectrum (- calculated, …. Experimental)

From the above spectrum, the ν_1 vibrational frequency is found to be 290(8) cm^{-1}. Here also a Zn-Cl increase of 0.095(5) Å with respect to the neutral ground

state. The spectroscopic constants of the $C^2\sum_g^+$ state are given in the following table together with other states of $ZnCl_2$.

	IPa (eV)[a]	IPv (eV)[b]	A (eV)[c]	$\omega_e(\nu_1)$ (cm^{-1})	$\omega_e(\nu_2)$ (cm^{-1})	r_{Zn-Cl} (Å)[d]
$X\ ^2\Pi_{g3/2}$		11.802 (5)			240 (20)	
$^2\Pi_{g1/2}$		11.880 (5)	0.078		260 (20)	
$A\ ^2\Pi_{u3/2}$		12.341 (10)		(360)	(280)	
$^2\Pi_{u3/2}$		12.451 (10)	0.110		(280)	
$B\ ^2\Sigma_u^+$		13.103 (15)				
$C\ ^2\Sigma_g^+$	14.065 (5)	14.101 (5)		290 (8)		2.145
3*d* bands						
$D\ ^2\Sigma_g^+$		19.037 (5)	19.037 (5)			
$E\ ^2\Pi_{g3/2}$		19.163 (5)	19.163 (5)			
$^2\Pi_{g1/2}$		19.434 (5)	19.434 (5)	0.271		
$F\ ^2\Delta_{g5/2}$		19.213 (6)	19.213 (6)			
$^2\Delta_{g3/2}$		19.499 (6)	19.499 (6)	0.286		

[a] Adiabatic ionization potentials.
[b] Vertical ionization potentials.
[c] Spin–orbit splitting parameters.
[d] Zn–Cl bond length. A bond length increase of 0.095(5) Å was obtained from the Franck–Condon factor calculation. The bond length in the neutral ground state is 2.05 Å from Ref. 7.

The spectrum of the 3d region of $ZnCl_2$ is shown in the following spectrum. This spectrum is useful to probe the bonding characters of the 3d orbitals in Zn.

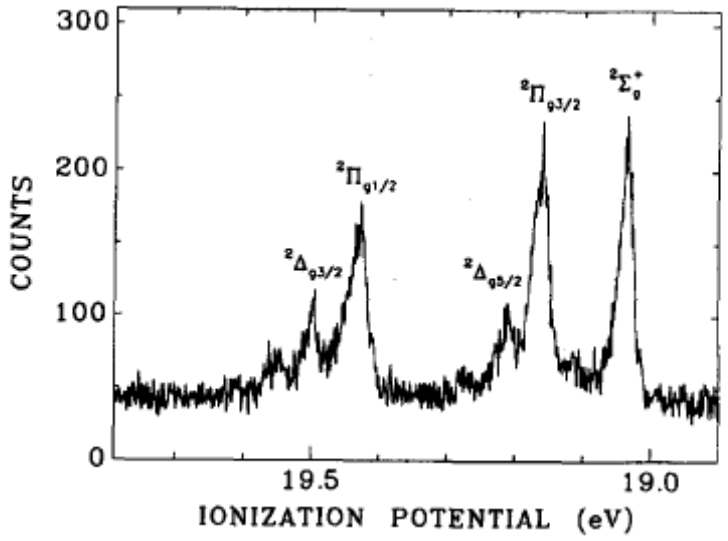

The photoelectron spectrum of $MnCl_2$

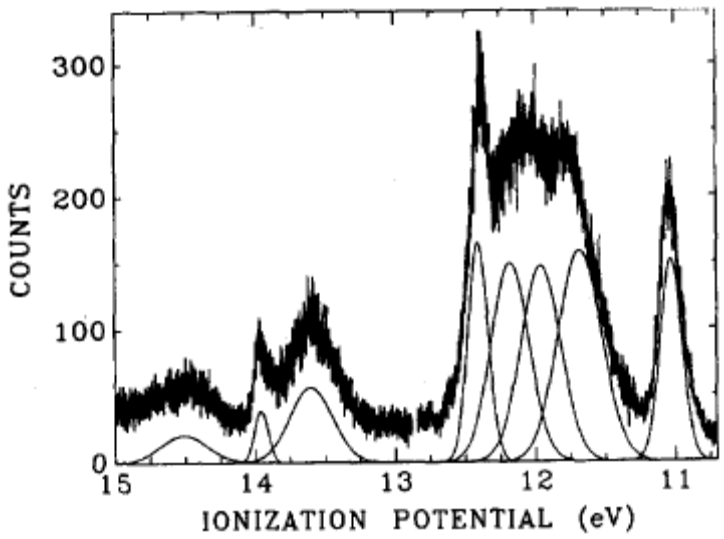

There are three relatively sharp bands at ionization energies of 11.03, 12.40, and 13.96 eV. The first two bands are assigned as being the d orbitals. The bands at 14.51, eV is due to low spin state from ionization of 8σg orbital. The three bands at ionization energies of 11.68, 11.96, and 12.18 eV are assigned to be from the 2πg, 4 πu, and $7\sigma_u$ orbitals, respectively. The three bands from d orbitals at 11.03, 12.40, and 13.96 eV are from the $9\sigma_g$, $3\pi_g$ and $1\delta_g$ orbitals respectively.

The overall assignments, the ionization energies, and the band widths from the Gaussian fitting of $MnCl_2$ are tabulated in the following table.

IP[a]	Assignment	Electronic term	FWHM (eV)[b]	Lee *et al.*[c]
11.03	$9\sigma_g^{-1}(3d)$	$^5\Sigma_g^+$	0.184	$9\sigma_g, 3\pi_g$
11.68	$2\pi_g^{-1}$	$^7\Pi_g$	0.367	$4\pi_u, 2u_g, 7\sigma_u$
11.96	$4\pi_u^{-1}$	$^7\Pi_u$	0.332	(did not
12.18	$7\sigma_u^{-1}$	$^7\Sigma_u^+$	0.314	specify)
12.40	$3\pi_g^{-1}(3d)$	$^5\Pi_g$	0.160	
13.60	$8\sigma_g^{-1}$	$^7\Sigma_g^+$	0.360	$1\delta_g, 8\sigma_g$
13.96	$1\delta_g^{-1}(3d)$	$^5\Delta_g$	0.115	(did not resolve)
14.51	$8\sigma_g^{-1}$	$^5\Sigma_g^+$	0.396	Satellite?

[a] Vertical ionization potentials, uncertainty = ± 0.01 eV.
[b] Full width at half-maximum of the fitted Gaussian.
[c] Reference 17.

The smaller splitting in $MnCl_2$ is due to the $8\sigma_g$ orbital can not overlap with the Mn 3d shell as much as a Mn 3s electron. The width and lower (than statistical, 5:7) relative intensity of the $^5\sum_g^+$ peak is analogous, which arises from the electron correlation.

The photoelectron spectrum of $NiCl_2$ in the gas phase

The spectrum is shown below :

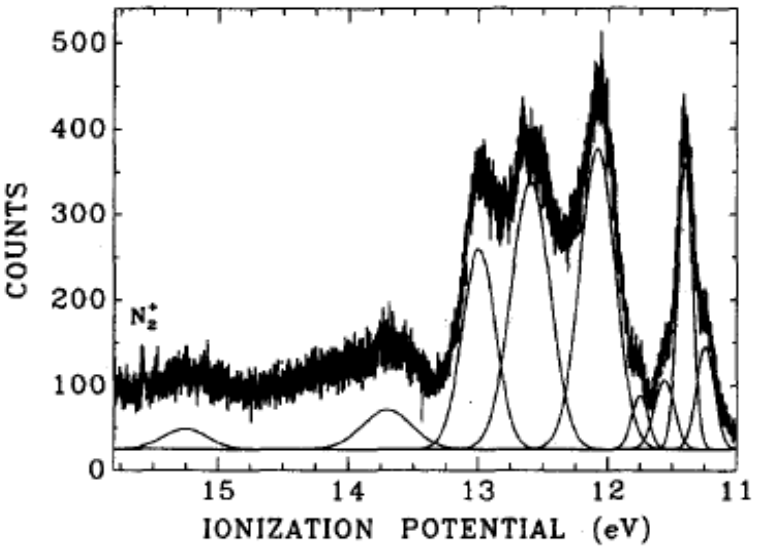

There are mainly four bands observed in the spectra which are from the d orbitals, on the basis of their small band widths. Some nitrogen impurity from the background at high ionization energy is observed. The rest of the spectrum can be assigned by analogous with those of $ZnCl_2$ and $MnCl_2$ as shown in the following table.

Ionization potentials (eV) and assignments for $NiCl_2$.

IP[a]	Assignment	Electronic term	FWHM (eV)[b]	Lee *et al.*[c]
11.24	$9\sigma_g^{-1}(3d)$	$^2\Pi_g$	0.166	$9\sigma_g, 3\pi_g, 1\delta_g$
11.40	$3\pi_g^{-1}(3d)$	$^4\Sigma_g^-$	0.135	(Only resolved
11.56	$1\delta_g^{-1}(3d)$	$^4\Phi_g$	0.183	one band)
11.76	$1\delta_g^{-1}(3d)$	$^4\Pi_g$	0.150	
12.08	$2\pi_g^{-1}$	$^4\Delta_g$	0.322	$4\pi_u, 2\pi_g, 7\sigma_u$
12.60	$4\pi_u^{-1}$	$4\Delta_u$	0.352	(did not
13.00	$7\sigma_u^{-1}$	$^4\Pi_u$	0.302	specify)
13.70	$8\sigma_g^{-1}$	$^4\Pi_g$	0.450	$8\sigma_g$
15.25	$8\sigma_g^{-1}$	$^2\Pi_g$	0.400	$3\pi_g$, Satellite?

[a] Vertical ionization potentials, uncertainty = ± 0.01 eV.
[b] Full width at half-maximum of the fitted Gaussian.
[c] Reference 17.

An expanded portion of the d region is plotted in the following figure

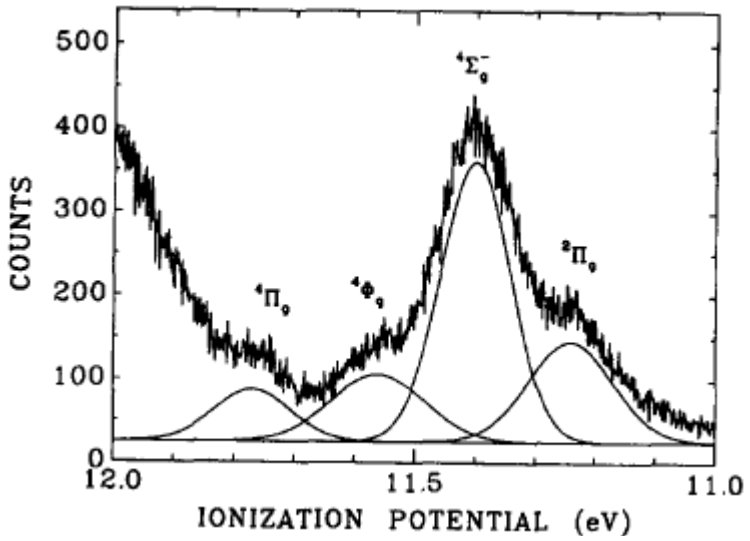

Here only four components are evident, by either visual inspection or curve fitting. Additional peaks may be present either coincident in energy or with low intensity. Some intensity is observed in ionization from each of the d orbitals, $9\sigma_g$, $3\pi_g$, and $1\delta_g$.

There are four spin-orbit components assigned for $NiCl_2$

$$\cdots 1\delta_g^4 3\pi_g^4 ({}^1\Sigma_g^+) \rightarrow \cdots 1\delta_g^4 3\pi_g^3, \quad {}^2\Pi_g \rightarrow {}^2\Pi_{g3/2}, {}^2\Pi_{g1/2}$$
$$\rightarrow \cdots 1\delta_g^3 3\pi_g^4, \quad {}^2\Delta_g \rightarrow {}^2\Delta_{g5/2}, {}^2\Delta_{g3/2}.$$

The observed four d bands could be assigned to the above four spin-orbit splitting parameters, 0.16 eV for the 2Πg state, and 0.20 eV for the $2\Delta_g$ state.

Electronic structure of $TiCl_4$ studied by XPS

High resolution x-ray photoelectron spectra of $TiCl_4$ in the solid state is compared with gas phase XPS data, UPS spectra, and theoretical models which shows specific characteristics of this molecular solids.

TABLE I. Electron binding energies in $TiCl_4$ in solid and gas phase (eV).

Levels		Solid (E_b^s)	Gas (E_b^g)	ΔE_b ($E_b^g - E_b^s$)
Ti	$2p_{1/2}$	464.4	471.5[a]	7.1
	$2p_{3/2}$	458.3	465.4	7.1
Cl	$2p_{1/2}$	199.5	207.7[a,b]	
	$2p_{3/2}$	198.0	206.6	8.6
Ti	$3p$	37.3	44.6[a]	7.3
Cl 3s	IV	17.3		
	III	15.9		
Ti–Cl bond II		6.0	13.2[c,d]	7.2
Cl lone pairs I		4.2	11.8	7.6

[a]XPS-g data from Ref. 2b.
[b]The Cl $2p$ spin orbit splitting is unusually small with respect to common observed values.
[c]UPS-g data from Ref. 1d.
[d]Weighted value of the $1t_1(\pi) - 2t_2(\sigma)$, $3t_2(\pi)$ lines binding energy, by taking into account the peaks area.

From this table we can concluded that the binding energy of $TiCl_4$ in gas phase is higer than solid phase. Further more, the binding energy for the small O1s contamination peak in $TiCl_4$, coincides with that in TiO_2 (E_b=530.3eV) the final product of $TiCl_4$ oxidation. In fact the absolute values of binding energies are not so important, as most of the discussion will be focused on comparisons between the gas and solid phases. The titanium ion is always tetrahedrally coordinated, but with slightly higer Ti-Cl distances in solid and the intramolecular Cl-Cl distances shorter in the solid phase.

X-ray photoelectron spectrum of Ti 2p levels of $TiCl_4$

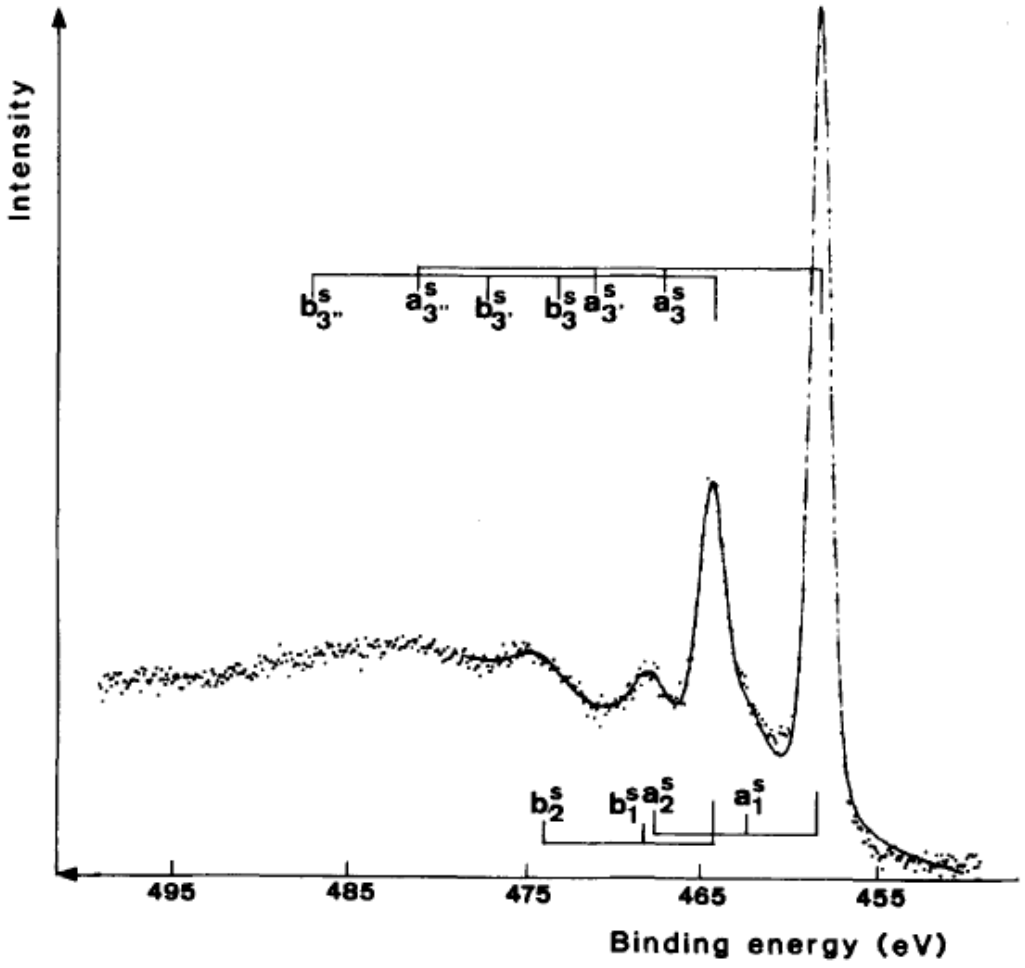

$TiCl_4$ belongs to the d^0 family, in these compounds there is no possibility for multiplet splitting due to a coupling between the metal core with unpaired d valance electrons. The Ti $2p_{3/2}$ and $2p_{1/2}$ satellites can then be expected to quite similar, especially in their number. Two satellites are found for Ti $2p_{3/2}$ (a_1^s,a_2^s) which are separated from the peak by 4.0 and 9.4 eV. The first satellites (b_1^s) is not resolved from the a_2^s satellites. The second Ti $2p_{3/2}$ is found at 9.7 eV from the main peak, with relative intensity greater than the corresponding value for Ti $2p_{3/2}$'s a_2^s satellite. The b_2^s satellite shows a shoulder on the low binding energy side. Finally beyond these resolved satellites, there is a broader peak at higher relative binding energy, whose position is difficult to define with precision because of the background shape in this region of the spectrum.

Applications :

- **Chemical-state analysis - Evaluates valence states, bonding environments, and the molecular composition of surface layers.**

- **Elemental analysis - Identifies elements from lithium to uranium, with detection levels down to 0.5%.**

- **Imaging -Uses faster scanning to produce images with a spatial resolution of 26 µm.**

- **Depth profiling - By sputtering material from a surface, generates compositional depth profiles for materials up to 1 µm thick.**

- **Thin-films - Frequently used for the analysis of surfaces of thin-film materials.**

- **Polymers - Especially valuable for analyzing functional groups in polymers and other organic materials. Particularly useful in this regard when used as a complementary tool with static SIMS analysis.**

- **Catalysts - Evaluates the surface of catalysts to determine reactive species.**

- **Other materials - Valuable for chemical-state analysis of materials ranging from metals to insulators to semiconductors.**

Summary:

Gas phase photoelectron spectra give accurate ionization energy of inorganic solids. Multiplet splitting of core electron binding energy can be obtained by this method from gas phase XPS we can know the specificity of the molecule in the condensed phase. From this we can know the interaction between metals with organic molecules in molecular level. By this technique we can know the structure and bonding of the inorganic cluster. The spin multiplicity of the corresponding state can be found out. Comparison of the photoelectron spectra obtained with different energy ionization sources provide insight concerning the amount of elemental character in the valence orbitals from which the ionizations arise. Gas phase studying of the molecules can avoid any possible disturbance from other species.

References:

1. T.Ishii *et al*., Physical Review., Vol.12, 1975

2. Christine Mousty-Desbequoite. *et al*. J.Chem.Phys. 79 (1), 1983

3. Lai sheng *et al*., J. Chem. Phys., Vol. 93, No. 2 (1990)

4. Lai-Sheng Wang *et al*.,*J. Phys. Chem.* 1996, *100,* 8697-8700

5. Dennis L. Lichtenberger, *et al*., *Inorg. Chem.* 1999, *38,* 4023

6. M. Copel, M. Gribelyuk, and E. Gusev, Appl. Phys. Lett. 76, 436 (2000)

7. M. Copel, M. Gribelyuk, and E. Gusev, Appl. Phys. Lett. 76, 436 (2000).

8. K. H. Bowen, Jr *et al*., J. Chem. Phys., Vol. 114, No. 22 (2001)

9. T. S. Jeon, J. M. White, and D. L. Kwong, Appl. Phys. Lett. 78, 368 (2001).

10. X. Yang, F. C. Jentoft R. E. Jentoft, F. Girgsdies, and T. Ressler, Catal Lett. 81(1-2), 25 (2002).

11. Nugent-Glandorf *et al*., Rev. Sci. Instrum., Vol. 73, No. 4 (2002)

12. Gerhards *et al*., J. Chem. Phys., Vol. 116, No. 23, 2002

13. Weijun Zheng, John M. Nilles, Owen C. Thomas, Kit H. Bowen Jr., Chemical Physics Letters 401 (2005), 266–270